Nonlinear optics as a probe of chiral ordering in amorphous semiconductors

D. P. DiVincenzo
IBM Research Division, Thomas J. Watson Research Center, P.O. Box 218, Yorktown Heights, New York 10598
(Received 22 June 1987)

Recent polytope models of amorphous semiconductors imply that the continuous random network has a preferred local chirality, that is, a preferred sign of the dihedral angle, extending over clusters of many atoms. The present work suggests an experimental test of this proposal. Symmetry arguments lead to two possible types of experiments: one involving local optical activity, and the other involving three-wave mixing. We present a detailed analysis of the latter: we show that a sensible definition exists for a local three-wave-mixing response of a single bond, develop a formalism for computing this local response within a tight-binding model, and perform computations that show that within a particular frequency regime (two high input frequencies above resonance and an output difference frequency below resonance) an experimentally detectable signal due to local chirality should be present.

I. INTRODUCTION

Some years ago a potentially powerful new concept emerged for the modeling of amorphous semiconductors. It began with the study of *polytopes*,[1-3] which are defined as undefected lattice structures ("crystals") in non-Euclidean space. Polytopes provide various motifs for possible favorable local atomic arrangements, like the icosahedral packing arrangement for close-packed systems[4-6] and the "twisted-boat" packing for tetrahedrally coordinated structures[7,8] (to be described in considerable detail later in this paper). However, the curvature of the space which contains them gives these motifs the property that they cannot be continued indefinitely; in a word, the atomic packings implied by polytopes are *frustrated*.[4,6] It was reasoned that the frustration of these packings, that is, the incompatibility of preferred local atomic arrangements with long-range order, could lead to disorder and provide a natural explanation for the occurrence of many types of disordered solids, as well as offering predictions for the properties of these solids.

The study of polytopes is a well-developed subject in mathematics.[3,9,10] It is essentially the consideration of Platonic solids and other regular figures in higher dimensions. Much discussion of the application of these polytopes to physics may be found in the literature, and I will not attempt to provide a complete review of this work here. Our work has its origins in the well-known efforts to apply the polytope $\{3,3,5\}$ to close-packed solids.[1,2,4-6] This polytope embodies the idea of perfect icosahedral close packing repeated throughout space; it can do this only by making space positively curved. So, as is well known, icosahedral packing is frustrated in real space. From this starting point, $\{3,3,5\}$ has been used to predict and explain the domain structure of disordered solids,[2,5] their structure factor,[11] the dynamics of glass formation,[12] and their relationship to complex crystalline phases like the Frank-Kasper phases.[1,2,4-6]

Modifications of polytope $\{3,3,5\}$ have figured in recent models of disordered semiconductors. The main principle of this modification, *decoration*,[13] is illustrated by the relationship between the fcc crystal, which describes close-packed solids, and the diamond lattice, which is a common structure for tetrahedrally coordinated, covalently bonded solids. The fcc crystal consists of a packing of octahedra and tetrahedra; if the tetrahedra (actually half of them) are "decorated" by placing one new atom at each of their centers, the diamond crystal results. Likewise when polytope $\{3,3,5\}$, which is a packing of all tetrahedra, is similarly decorated (in this case one in every five tetrahedra is decorated), a new structure[14] which has been termed "polytope 240"[13,15] results which has many promising features for describing a tetrahedrally coordinated network.

Polytope 240 has perfect tetrahedral bond angles and bond lengths. The rings of bonds in the structure are all six membered, which is also true of the most common crystalline modifications of the group-IV elements. However, beyond this there are differences between polytope 240 and ordinary crystals. At the root of the difference lies the fact that the six-membered ring is "nonrigid," i.e., has an infinite number of configurations which are consistent with the bond lengths and bond angles of the tetrahedral structure.[16,7,8] Two of these configurations have been known for a long time and occur commonly in tetrahedral crystals: the so-called "boat" and "chair" rings (see Fig. 1). The remaining infinite set of configurations can be obtained from the "boat" geometry by continuous deformation, which we have discussed before;[8] this continuous deformation can be parametrized by a number which we have termed the "twist" (see Fig. 2). Polytope 240 is the realization of a perfect packing of six-membered rings with a particular value of this twist.

An equivalent description for this structural freedom provided by this "ring nonrigidity" may be given in terms of the "dihedral angles" of the network. The dihedral angle ϕ is defined in Fig. 3; while in crystals ϕ is generally either staggered ($\phi=60°$) or eclipsed ($\phi=0°$), in the continuous random network ϕ can assume any value. The twisted six-membered rings sample the entire

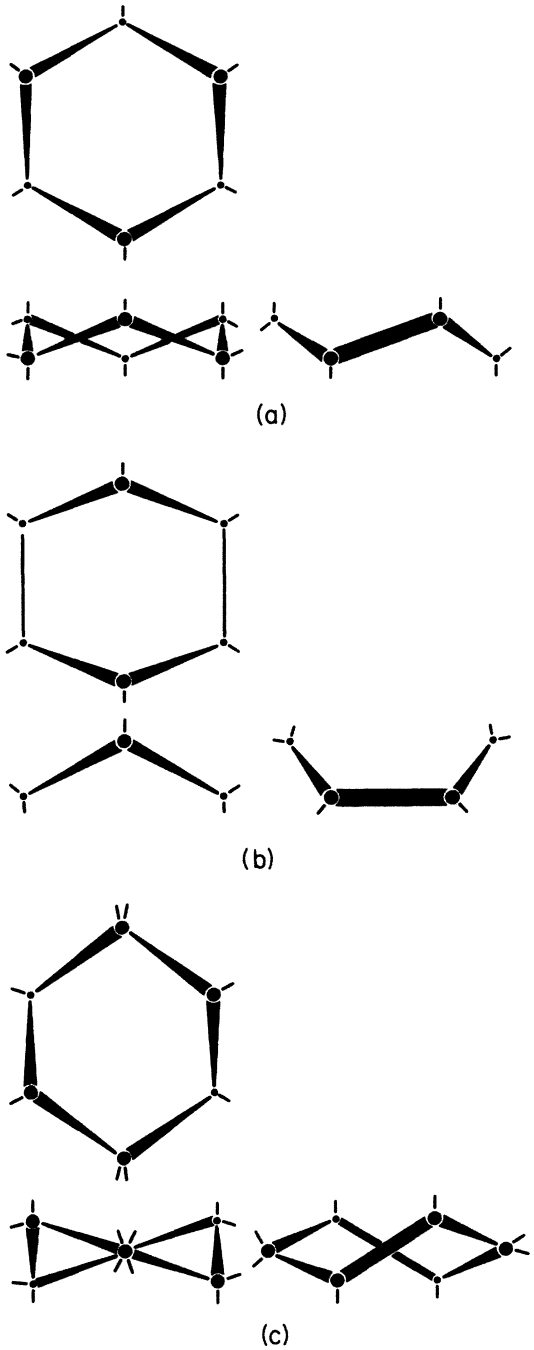

FIG. 1. Different conformations of six-membered rings, shown in top, front, and side views: (a) "chair," (b) "boat," (c) "twisted boat." The last can be obtained from the ordinary boat by a continuous deformation involving no bond angle or bond length changes.

range of dihedral angles.

Part 1 of the Appendix discusses the symmetry properties of these twisted rings. A "boat" ring with a noncrystallographic value of twist (i.e., $\phi \neq 0°, 60°$) has no symmetries except for a twofold rotation axis. These rings have no mirror symmetries, meaning that twisted rings come in enantiomorphous pairs. There is a distinguishable "left" and "right" handed version of each ring.

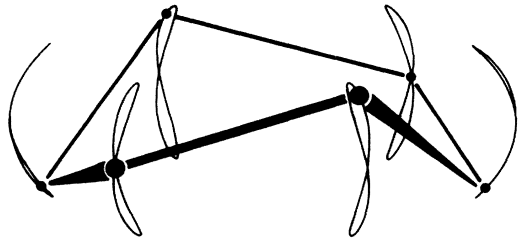

FIG. 2. The twist degree of freedom of the "boat" ring. The atoms can slide around the figure-eights with no distortion of the bond lengths or bond angles.

An equivalent way of saying the same thing in terms of the dihedral angle ϕ is that each bond has a distinct handedness which may be assigned according to whether ϕ is positive or negative.[17]

This is what is meant by the "local chirality" of the covalent network: the chirality of a bond is determined by the dihedral angle ϕ. When $\phi = -60°, 0°, 60°$, etc., the local arrangement of atoms has a mirror symmetry, and is not chiral. We can say that for $-60° < \phi < 0°$, the bond is "left-hand chiral," and for $0° < \phi < 60°$ it is "right-hand chiral." In polytope $\{3,3,5\}$, all the dihedral angles are the same, about $+30°$ (because each six-membered ring has the same value of the ring twist), so the structure has a net chirality. As we will see below in more detail, nonlinear light scattering will measure the volume over which the bond chirality has the same sign.

Motivated by this intriguing property, Sachdev and Nelson[18] examined the Connell-Temkin model[19] for large-scale chirality. The Connell-Temkin model is a hand-built structure which attempted to simulate the continuous random network structure of amorphous semiconductors. *A priori* it has a better chance than many other similar models to share properties with polytope 240, because it is constrained to contain only even-membered rings. Sachdev and Nelson found that this model does indeed contain a bias towards a single chirality over a large fraction of the model. (The model contains 243 sites.) This observation (later confirmed more quantitatively by analysis which we performed[8] on the Connell-Temkin and other models) stimulated a hypothesis: that in real amorphous semiconductors the structure may prefer having a local chirality, and that the sign of the chirality will persist over clusters of perhaps 100 atoms (i.e., some reasonable fraction of the number of atoms in polytope 240).

This hypothesis, if true, would have significant implications for the presence of intermediate-range order in

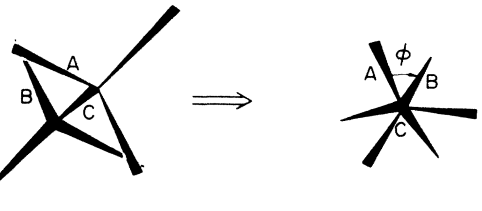

FIG. 3. The dihedral angle ϕ for a bond in a tetrahedral network. ϕ is the angle between the second-neighbor bonds A and B when viewed along the connecting bond C.

amorphous semiconductors. It implies the existence of a length scale which has not been previously considered, the radius of curvature of the polytope,[4] which would extend over several interatomic spacings (four or five). Unfortunately, the hypothesis rests on rather unfirm ground. We know almost nothing about the actual microscopic processes which form the amorphous network and whether they have any kinship to hand-built random network models. The Connell-Temkin model possesses significant polytope order, but it was built with the constraint that all of the rings of bonds be even membered. Several other successful models due to Polk[20,21] and Wooten *et al.*,[22] built without an even-ring constraint, seem to show very little polytope order. We do not know if even-membered rings are favored by the microscopic growth mechanisms; we do not know if even-membered rings are necessary for the appearance of polytope order. Nevertheless, the possibility of local chirality in amorphous networks is an intriguing suggestion. It is one which deserves to be tested; the central purpose of this paper is to suggest a method by which this test may be made.

Higher-order structural correlations have not been an easy property to probe in amorphous solids. X-ray scattering gives just the atom-atom correlation functions; these contain little or no information about ring twist or dihedral angles. We have been motivated to search for a method of extracting this information in the area of nonlinear optics by a consideration of some general features of the optical response of solids. First, the method chosen must be capable of extracting *local* properties of the solid; light scattering, being sensitive to two-point correlation functions,[23–26] can fill this role.[27] However, in the present case, the local property is a peculiar one, "chirality." What makes it peculiar is that, from the point of view of symmetry, chirality is a *pseudoscalar,* meaning that its value changes sign under mirror reflection. This is an unusual physical property, making it distinct from, for example, the atom density, which is a true scalar. In the linear regime the magnitude of light scattering is controlled by a rank-two tensor, the dielectric matrix.[23] This matrix contains a true scalar part (its trace), meaning that light scattering can probe fluctuations in atom density, as indeed it does in Rayleigh scattering. The dielectric tensor[23] does not contain a pseudoscalar component, meaning that it is impossible for linear light scattering to be sensitive to local chirality.

This requires that the search for an acceptable technique be extended to higher-order optical processes, ones described by tensors with rank greater than two. On general grounds we know that only odd-rank tensors can change sign under inversion, so we search only among this set. Naturally we wish to keep the resulting technique as simple as possible, and this finally confines us to consider optical effects which are described by rank-three tensor responses.

Two such phenomena will be considered in this paper.

1. Three-wave mixing.[28] Phenomenologically, this is described by the second term of the power-series expansion of the induced polarization of the solid in terms of the applied electric fields:[29]

$$P_i = \chi_{ij} E_j + \beta_{ijk} E_j E_k + \cdots . \tag{1}$$

In various limits, it describes *second-harmonic generation,* in which radiation of frequency ω impinging on a solid causes the production of radiation at frequency 2ω, as well as the *electro-optic effect,*[30] in which an applied static electric field induces a change in the dielectric response (i.e., index of refraction) in a material. In the general case, two different radiation fields at two different frequencies ω_1 and ω_2 will produce radiation at the sum and difference frequencies because of the three-wave mixing phenomenon. In this paper we analyze in detail an experimental situation which corresponds approximately to the inverse of the electro-optic effect.

2. Optical activity.[30,31] This phenomenon results from spatial dispersion of the dielectric response:

$$P_i = \chi_{ij} E_j + g_{ijk} q_j E_k + \cdots . \tag{2}$$

In other words, optical activity follows from the dependence of the dielectric polarizability on the wave vector **q** of the incident radiation. Left-circular-polarized and right-circular-polarized radiation are distinguishable only with respect to the direction of the light's wave vector **q**, so any difference in the response of a solid to left- and right-circular polarization must result from optical activity.

In materials with a net left or right handedness, these two phenomena can be used in a straightforward way to detect the presence of chirality.

(1) Consider applying a circularly polarized electric field in the x-y plane. Because of the three-wave mixing response, the chiral medium will develop a net polarization along the z axis. Figure 4 shows this experiment where the chiral "medium" is a wire coil; the electrons move along the coil, creating a polarization, in much the same way that a fluid moves along an Archimedean screw.[32] The illustrated phenomenon is a degenerate case of a three-wave mixing, because the two input waves (the x and y components of the incident field) are at the same frequency, while the output wave, the resultant polarization vector, is at zero frequency. This may be termed an inverse electro-optic effect, since the static

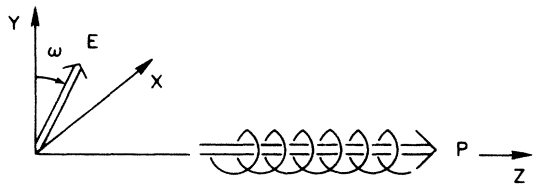

FIG. 4. Illustration of a classical nonlinear electrical phenomenon which is sensitive to chirality. If a helical wire is placed in a uniform time-dependent electric field with a circular polarization in the x-y plane as shown, the helix will develop a frequency-independent polarization along its axis. The sign of the polarization depends on the chirality of the coil, that is, whether it is left or right handed. We expect this phenomenon to be too weak to be measured in a benchtop experiment, but it can be important on a microscopic scale.

field, rather than influencing the finite-frequency excitation, is produced by it.

(2) The method used to detect optical activity is probably more familiar to the reader. If a beam of linearly polarized light is passed through the chiral medium, the polarization of the emergent beam, while still linear, is rotated with respect to the incident polarization. This is a consequence of the distinction between left and right circularly polarized radiation; in particular, of their having different group velocities. The incident linearly polarized beam may be viewed as an equal linear combination of left and right circular polarization; when these two components pass through the solid, the phase of one lags relative to the other, so that upon recombining after emerging from the solid, the orientation of the linear polarization is rotated.

Neither of the two techniques just described is useful for probing a medium which contains many domains with random left- and right-hand chirality. In the first example the local induced polarization will have random sign, so that the net polarization is zero, and in the second case, each region will rotate the passing radiation's polarization but with a random sense, so the net rotation is zero. However, modifications of these experiments can be devised which will detect the presence of chirality even in the random-domain case.

(1) Here is an appropriate modification of the inverse electro-optic experiment described above. Suppose that the two incident beams in the x- and y-polarization channels, rather than being at the same frequency, are at slightly displaced frequencies ω and $\omega+\Delta\omega$. The x wave will be continuously phase shifted with respect to the y wave, so that the polarization state will vary continuously from right circular to right elliptic to linear to left elliptic to left circular and back again with a frequency $\Delta\omega$. As the polarization varies from right to left circular, the sign of the induced polarization will reverse, also at frequency $\Delta\omega$. So, we have managed to create inside the medium a time varying, spatially fluctuating polarization distribution. This is precisely the situation in Rayleigh scattering;[23] the difference is that in Rayleigh scattering the spatially varying polarization is produced by the *linear* interaction of the incident radiation with density fluctuations in the medium. In the Rayleigh-scattering case, of course, the frequency is the same as that of the incident light.

The final product of this experiment is the incoherent radiation which is produced from this ensemble of randomly oriented dipoles; this is completely analogous to the blue sky produced by Rayleigh scattering. As with Rayleigh scattering, the magnitude of the radiation produced is in direct proportion to the coherence length, that is, to the size of the coherently radiating regions. In the three-wave mixing case this length is precisely the chirality persistence length, which is the primary quantity of interest. Of course, the size of the effect must also depend on some microscopic coupling constant, which we will estimate later in this paper. We find that although the predicted magnitude of the three-wave mixing effect is small, it should be observable using state-of-the-art laser techniques and should consequently be able to provide a direct measurement of the chirality persistence length.

(2) Optical activity can also be used indirectly to probe the chirality persistence length. As mentioned above, optical activity results from the difference in group velocities of left- and right-circular polarized light. Complementary to this phenomenon (related to it through the Kramers-Kronig formula, in fact) is the difference in absorption coefficients for the two circular polarizations. In principle one could imagine a spectral regime in which the absorption coefficient for left circularly polarized light of the left chiral regions is very high, while that of the right chiral region is very low. A very intense pulse may then result in a very highly excited carrier distribution in the left chiral regions, leaving a lower-energy carrier distribution in the right chiral regions. This could, for a short time, leave the left chiral regions saturated, so that another linearly polarized pulse might respond only to the right-hand regions and so be rotated. The time scale for the decay of this effect is hard to predict, but it should be related to the time required for highly excited carriers to diffuse from left-chiral domains to right-chiral domains. Thus it should be a monotonic function of the size of these domains. Related polarization-memory measurements have been performed for linear polarization in crystalline materials.[33] In this case the decay times are observed to be on the order of hundreds of femtoseconds; however, the decay mode is quite different, being related to momentum-space relaxation of high-energy carriers rather than real-space relaxation. An interesting future calculation would involve setting up a high-energy carrier Boltzmann equation to attempt to estimate this decay time theoretically.

Random spatial variations in optical activity cause the material to produce diffusely scattered light; thus, one might think that method (1) above could be used to detect local chirality via optical activity. However, we advise against this for the following reason. Optical activity is linear with regard to field strengths; frequencies are left unchanged. Thus although optical activity *does* produce diffuse scattered light, it is at the same frequency and thus very difficult to distinguish from ordinary Rayleigh-scattered light. Conversely, there is a good reason that we do not propose a selective-saturated scheme in conjunction with the three-wave mixing phenomenon. Since three-wave mixing is nonlinear, the polarization vector $\mathbf{P}$ and the electric fields $\mathbf{E}$ are at different frequencies, so that the time-averaged power produced by $\mathbf{P}(t)\cdot\mathbf{E}(t)$ is zero. Therefore, three-wave mixing cannot contribute to energy absorption in the solid.

II. MICROSCOPIC CALCULATION

As mentioned above, some estimate is needed for the microscopic three-wave mixing response. To the greatest extent possible we wish this calculation to characterize the *local* response of the material, since we are interested in seeing how well this local response cor-

responds with the local chirality, i.e., the local dihedral angle.

In covalent materials it is natural to break up the physical response into local contributions from individual bonds. The general idea, which has actually been applied by Harrison[34] and others[35–37] to compute similar optical coefficients, is to assume that the charge in the bond will be polarized by an external field, producing a dipole moment which may depend nonlinearly on the incident field strength. To estimate this dipole, Harrison[34] constructs the simplest possible quantum-mechanical model for the bond: a two-level-system description, the two levels being the bonding and antibonding levels. Harrison finds that the volume density of nonlinear polarizability β is roughly given by

$$\beta \sim \frac{e^3}{E_{\text{gap}}^2} . \tag{3}$$

Here e is the electron charge and E_{gap} is some average energy band gap. We will show in more detail below how an expression of this sort is derived. This equation predicts an approximate magnitude for the nonlinear response of about $\beta/e^3 \sim 0.1\ (\text{eV})^{-2}$. This will turn out to be about right. However, the simple Harrison approach to this calculation is inadequate in the following several respects.

(1) An honest evaluation of the polarizability β_{ijk} in Harrison's approximation gives zero for a homopolar semiconductor like Si or Ge. This is so because in the approximation in which the homopolar bond is an isolated two-level system, it has an inversion symmetry, so that every odd-rank tensor property must vanish.

(2) Harrison's method of estimating β is only appropriate in the $\omega \rightarrow 0$ limit; the inverse electro-optic phenomenon of interest will vanish in this limit, even if the inversion-symmetry approximation is not made.

A more extended theory than Harrison's is required to provide a real estimate of β. We have devised a model which remedies both these deficiencies, the first by including the influence of a bond's environment on its polarizability (necessary so that the bond's response can be sensitive to the local network's chirality), and the second by evaluating the full frequency-dependent expression for β_{ijk} rather than just its static limit.

We have taken into account the environment of each bond by embedding each bond in an extended cluster, numbering typically 20–30 Si atoms with H terminations on the outer bonds. We make these clusters by extracting subclusters of various regions of two hand-built models of the continuous random network mentioned above, the Connell-Temkin model[19] and the Polk model.[20] We have studied the entire ensemble of clusters so generated, which permits us below to get valuable information on the spatial distribution of three-wave mixing response in these networks, which we discuss later. The cluster sizes were chosen so that all rings up to a certain size which included the bond of interest were kept; we experimented with keeping up to six-membered rings and up to eight-membered rings.

The full frequency-dependent expression for the three-wave mixing polarizability β_{ijk} is most conveniently derived by perturbation theory applied to the density matrix of the system starting with the Heisenberg equation of motion. Shen has presented a correct derivation of this sort.[28] The perturbation to the system may be represented by a scalar electric potential:

$$\phi(r,t) = e\mathbf{r}\cdot\mathbf{E}_1 e^{i\omega_1 t} + e\mathbf{r}\cdot\mathbf{E}_2 e^{i\omega_2 t} . \tag{4}$$

Note that we can work in a gauge in which the vector potential is zero, so that the whole perturbation is in the scalar potential ϕ. It is possible to use this gauge because we make the long-wavelength approximation (setting the wave vector to zero), in which the magnetic field vanishes. It is the most convenient gauge for constructing a consistent theory for clusters within a tight-binding approximation; for crystalline solids another gauge is appropriate (see the Appendix, part 3). The effect of this perturbation is evaluated to second order, and we determine how it changes the expectation value of the dipole moment of the bond; we denote the quantum operator measuring this quantity $\hat{r}_i^{\text{bond}}$. We will describe the exact meaning of this operator a little later.

The expression so obtained by Shen[28,28] goes like

$$\beta_{ijk}(\omega_1,\omega_2;\omega=\omega_1+\omega_2) = \frac{-e^3}{V^{\text{bond}}\hbar^2} \frac{(\hat{r}_i^{\text{bond}})_{gn}(\hat{r}_j)_{nn'}(\hat{r}_k)_{n'g}}{(\omega-\omega_{ng}+i\Gamma_{ng})(\omega_2-\omega_{n'g}+i\Gamma_{n'g})} + (7 \text{ more terms}) . \tag{5}$$

V^{bond} is the volume per bond in the solid; note that as expected this expression has the units e^3/eV^2. Matrix elements are between the many-electron states of the system; g denotes the ground state, n and n' denote excited states. The other seven terms of this expression are given on p. 17 of Shen; to convert these to our notation, replace Shen's $\hat{r}_i$ with my $\hat{r}_i^{\text{bond}}$ and Shen's N with my $1/V^{\text{bond}}$. (We are computing the response per unit volume rather than the total response.) Using the frequency convention of Eq. (5), the *difference*-frequency response is represented by ω_1 or $\omega_2 < 0$.

The dipole-moment operators $\hat{r}_i$ and $\hat{r}_i^{\text{bond}}$ require some discussion. The many-electron matrix elements required in Eq. (5) are evaluated in the usual way:

$$(\hat{r}_i)_{\text{ab}} = \int\int\cdots\int \prod_\alpha d\mathbf{r}_\alpha \Psi_a^*(\{r_\alpha\})\hat{r}_i(\{r_\alpha\})\Psi_b(\{r_a\}) . \tag{6}$$

Ψ is the fermion wave function. The operator $\hat{r}_i$, the dipole operator in the ith Cartesian direction, is a simple one-particle operator[38,39] which can be written as follows:

$$\hat{r}_i = \int_{\text{all space}} \mathbf{n}_i\cdot\mathbf{r}\hat{\rho}(\mathbf{r})d\mathbf{r} . \tag{7}$$

(Here $\mathbf{n}_i$ is the unit vector in the ith Cartesian direction.) Here $\hat{\rho}$ is the one-particle density operator

$$\hat{\rho}(\mathbf{r})=\sum_{\alpha}\delta(\mathbf{r}-\mathbf{r}_{\alpha}) .$$

The α sum runs over the electrons in the system. Note that the matrix elements of the operator $\hat{r}_i$ are to be evaluated over the whole cluster; in this way Eq. (5), which gives the response of a single bond, is influenced nonlocally by the entire neighborhood of that bond.

One might expect the "bond dipole-moment operator" $\hat{r}_i^{\text{bond}}$ to be given by an expression similar to Eq. (7) with the integral over all space replaced by an integral just over the volume of the bond:

$$\hat{r}_i^{\text{bond}} \stackrel{?}{=} \int_{|\mathbf{r}-\mathbf{r}_0|\le|\mathbf{R}|} n_i\cdot\mathbf{r}\hat{\rho}(\mathbf{r})d\mathbf{r} . \tag{8}$$

We imagine that the "bond" region is defined by a sphere of radius $|\mathbf{R}|$ centered on the middle of the bond $\mathbf{r}_0$. Equation (8) is almost correct, but it is unsatisfactory because it depends on the position of the bond $\mathbf{r}_0$. The problem is that the perturbation to the bond will in general acquire a monopole moment because of charges flowing in and out from neighboring bonds. As in classical electricity,[40] the dipole moment is well defined only in the absence of a monopole. We can cure this problem by subtracting away the monopole moment of the bond:

$$\hat{r}_i^{\text{bond}}=\int_{|\mathbf{r}-\mathbf{r}_0|\le\mathbf{R}}\mathbf{n}_i\cdot\mathbf{r}\,d\mathbf{r}\left[\hat{\rho}(\mathbf{r})-\frac{1}{V^{\text{sphere}}}\times\int_{|\mathbf{r}'-\mathbf{r}_0|\le\mathbf{R}}\hat{\rho}(\mathbf{r}')d\mathbf{r}'\right]. \tag{9}$$

Here $V^{\text{sphere}}=\frac{4}{3}\pi\mathbf{R}^3$. While Eq. (9) may appear somewhat *ad hoc*, it is no more so than Harrison's approach[34] which eliminates the monopole by completely decoupling one bond from another, removing the possibility of intrabond charge flow. Equation (9) may be rewritten in a convenient equivalent form:

$$\hat{r}_i^{\text{bond}}=\sum_{\alpha}\mathbf{n}_i\cdot(\mathbf{r}_{\alpha}-\mathbf{r}_0)\theta^{\text{bond}}(\mathbf{r}_{\alpha}) , \tag{10}$$

where

$$\theta^{\text{bond}}(\mathbf{r})=\begin{cases}1, & |\mathbf{r}-\mathbf{r}_0|\le|\mathbf{R}|\\ 0, & \text{otherwise} .\end{cases} \tag{11}$$

There is another possible approach to this calculation in which, instead of computing the induced dipole moment at the bond, we can compute the current density integrated over the bond region. Then, at finite frequency the current is related to the induced polarization by[41]

$$\mathbf{J}=\frac{d\mathbf{P}}{dt} . \tag{12}$$

We have not performed any computations using this approach; we expect that it would have given qualitatively very similar results. Part 3 of the Appendix mentions some details of how this scheme might be implemented, and some complications of using the current formalism within the tight-binding approximation which ultimately discouraged us from using it; it would be necessary to use this alternative formalism in infinite crystals, however.

Now we review how the above calculations are done in the tight-binding limit.[42–44] First, tight-binding implies that we work in the approximation of noninteracting electrons. In this case, the ground state g is a single Slater determinant; since the dipole operators in Eq. (5) are all single-particle operators, the states labeled n and n' must both be one particle-one hole states. There are two distinct possibilities: either n and n' involve the same particle states and (in general) different hole states, or vice versa. Evaluating Eq. (5) in terms of single-particle eigenstates, we obtain

$$\beta_{ijk}(\omega_1,\omega_2;\omega=\omega_1+\omega_2)=\frac{-e^3}{V^{\text{bond}}\hbar^2}\sum_{\alpha,\beta,\gamma}f_{\alpha}(1-f_{\beta})(1-f_{\gamma})\frac{\langle\alpha|\hat{r}_i^{\text{bond}}|\beta\rangle\langle\beta|\hat{r}_j|\gamma\rangle\langle\gamma|\hat{r}_k|\alpha\rangle}{(\omega-\omega_{\beta\alpha}+i\Gamma_{\beta\alpha})(\omega_2-\omega_{\gamma\alpha}+i\Gamma_{\gamma\alpha})}$$
$$+(15\text{ more terms}) . \tag{13}$$

α, β, and γ denote the one-particle eigenstates, and f_{α} is the Fermi function. Part 2 of the Appendix contains more details about this expression, which, so far as we can tell, has not been correctly obtained previously in the literature. (For example, Shen's expression[28] [his Eq. (2.18)] is wrong.) $\hat{r}_i$ and $\hat{r}_i^{\text{bond}}$ now denote the single-particle versions of the dipole operator, which by using Eqs. (7)–(11) and using the usual rules[39] are given by

$$\hat{r}_i=\mathbf{n}_i\cdot\mathbf{r} , \tag{14}$$

$$\hat{r}_i^{\text{bond}}=\mathbf{n}_i\cdot(\mathbf{r}-\mathbf{r}_0)\theta^{\text{bond}}(\mathbf{r}) . \tag{15}$$

The eigenstates $|\alpha\rangle$ are obtained as eigenvectors of a standard tight-binding model Hamiltonian for Si, which has been discussed by many other authors.[43–45] The particular form of the Hamiltonian we use has been taken from the work of Alerhand, Mele, and Allan.[42,46,47] By diagonalizing this Hamiltonian we obtain the eigenstates as linear combinations of tight-binding basis functions:

$$|\alpha\rangle=\sum_{i,\mu}a_{i\mu}|\phi_{i\mu}\rangle . \tag{16}$$

$|\phi_{i\mu}\rangle$ are the basis functions, orbitals centered on atom i with angular momentum quantum number labeled by μ (s,p_x,p_y,p_z).

Substituting Eq. (16) into Eq. (13), we find that the only additional piece of information which is required to complete the calculation is the value of the orbital matrix elements $\langle\phi_{k\mu}|\hat{r}_i|\phi_{l\nu}\rangle$ and $\langle\phi_{k\mu}|\hat{r}_i^{\text{bond}}|\phi_{l\nu}\rangle$. For $\hat{r}$ we use the usual approximation of tight-binding theory:[42]

$$\langle\phi_{k\mu}|\hat{r}_i|\phi_{l\nu}\rangle=\delta_{kl}\delta_{\mu\nu}(R_i)_k \ . \tag{17}$$

Here $(R_i)_k$ is the ith Cartesian component of the position vector of atom k. Equation (17) implies that the basis functions are eigenfunctions of the dipole operator:

$$\hat{r}_i|\phi_{l\nu}\rangle=(R_i)_k|\phi_{l\nu}\rangle \ . \tag{18}$$

Finally, we need to evaluate

$$\langle\phi_{k\mu}|\hat{r}_i^{\text{bond}}|\phi_{l\nu}\rangle=\mathbf{n}_i\cdot(\mathbf{R}_k-\mathbf{r}_0)\langle\phi_{k\mu}|\theta^{\text{bond}}|\phi_{l\nu}\rangle \ , \tag{19}$$

where

$$\langle\phi_{k\nu}|\theta^{\text{bond}}|\phi_{l\mu}\rangle\equiv\int_{\text{bond}}\phi_{k\mu}(\mathbf{R})\phi_{l\nu}(\mathbf{R})d\mathbf{R} \ . \tag{20}$$

We make the following approximation to the θ^{bond} matrix element:

$$\langle\phi_{k\mu}|\theta^{\text{bond}}|\phi_{l\nu}\rangle=\begin{cases}\frac{1}{4}\delta_{kl}\delta_{\mu\nu}, & \text{atom } k \text{ in bond}\\ 0, & \text{otherwise} \ .\end{cases} \tag{21}$$

We take the matrix element to be one-quarter of the normalization integral since each atom is shared among four bonds. This choice satisfies the constraint that the θ matrix element, summed over all bonds, gives the identity operator. (This is implied by the relation $\sum_{\text{bond}}\hat{r}_i^{\text{bond}}=\hat{r}_i$.) Many other choices are of course possible, but we do not expect the physics to be qualitatively altered by this choice.

III. RESULTS

Using Eq. (13), we have evaluated the three-wave mixing polarizability β_{ijk} for Si—Si bonds in a random network environment. Before plunging into the full complexity of the realistic system, we show in Fig. 5 a contour plot of β for a simple two-level system. We have shown one particular component of the β_{ijk} tensor, namely the piece which is fully antisymmetric with respect to interchange of tensor indices. This can be extracted from the full tensor by contracting it with the fully antisymmetric (Levi-Cività) third-rank tensor: $\beta_a\equiv\epsilon_{ijk}\beta_{ijk}$. Since ϵ_{ijk} is a pseudoscalar, this operation projects out the pseudoscalar component of β_{ijk}. As discussed in the Introduction, this is the part of the three-wave mixing response which we expect to be sensitive to network chirality. The symmetry properties of $\beta_a(\omega_1,\omega_2;\omega=\omega_1+\omega_2)$ are illustrated by Fig. 5, which shows the calculation of β_a for a two-level system. These symmetries are obtained from the following two relations which are true for the full three-wave mixing tensor:

$$\begin{aligned}&\beta_{ijk}(\omega_1,\omega_2;\omega)=\beta_{ikj}(\omega_2,\omega_1;\omega) \ ,\\ &\beta_{ijk}(\omega_1,\omega_2;\omega)=\beta_{ijk}^*(-\omega_1,-\omega_2;-\omega) \ .\end{aligned} \tag{22}$$

When contracted with ϵ_{ijk}, this gives the following relations for the fully antisymmetric response:

$$\begin{aligned}&\text{Re}\beta_a(\omega_1,\omega_2;\omega)=-\text{Re}\beta_a(\omega_2,\omega_1;\omega) \ ,\\ &\text{Im}\beta_a(\omega_1,\omega_2;\omega)=\text{Im}\beta_a(\omega_2,\omega_1;\omega) \ ,\\ &\text{Re}\beta_a(\omega_1,\omega_2;\omega)=\text{Re}\beta_a(-\omega_1,-\omega_2;-\omega) \ ,\\ &\text{Im}\beta_a(\omega_1,\omega_2;\omega)=-\text{Im}\beta_a(-\omega_1,-\omega_2;-\omega) \ .\end{aligned} \tag{23}$$

As the figure illustrates, these relations imply $\text{Re}\beta_a(\omega_1,\omega_1;2\omega_1)=0$—there is no antisymmetric component to the second-harmonic response.[28] On the other hand, the response β_a is nonzero when $\omega_1=-\omega_2$, and in fact this is the response which we described in the Introduction and which we study in detail below. Its phase is fixed, since its real part is zero.

The overall frequency dependence of the antisymmetric response is determined by symmetry properties and by the resonant structure of the energy denominators, which cause the response to have structure along the lines $\omega_1=\pm\omega_{\text{gap}}$, $\omega_2=\pm\omega_{\text{gap}}$, and $\omega_1-\omega_2=\pm\omega_{\text{gap}}$ (see Fig. 5).

The antisymmetric response of an actual Si—Si bond randomly chosen from inside the Connell-Temkin model is shown in Fig. 6. In its overall spectral distribution, it resembles the two-level case, except that the resonant structure is spread over a somewhat larger band. The average resonant frequency is about 6 eV as for the linear dielectric function. We expect our tight-binding model to give a fairly reliable picture of the general resonant structure of the polarizability, but not faithfully to represent the real frequency scales in the actual solid, nor faithfully to apportion oscillator strengths among various parts of the optical band. This will be satisfactory, since we will only demand qualitative information from these calculations. Note that the maximum size of the three-wave mixing is about 0.01 $(\text{eV})^{-2}$; this is typical of all the bonds from the Connell-Temkin or Polk models, with a wide variation of about an order of magnitude. Thus, the crude estimate of 0.1 $(\text{eV})^{-2}$ given in the Introduction, while perhaps a bit optimistic, is not unrealistic.

We focus on the inverse electro-optic limit of the response, that is, near the line $\omega_1=-\omega_2$ in Fig. 6. The key question is, does the sign of the inverse electro-optic response of a bond faithfully reflect the local chirality (i.e., the sign of the dihedral angle) at that bond? As discussed earlier, only features of the bond's environment which break inversion symmetry can result in a nonzero response; therefore, the dihedral angle at that bond is certainly one of the possible structural parameters which can contribute. However, there are others. For exam-

ple, fluctuations in bond angle can also contribute to the local breaking of inversion symmetry. Probably a more important complicating factor is that the bond polarizability is not very local, and can depend on the geometry of the network farther from the bond—on topological disorder related to the ring statistics, for example. We shall see that there is a frequency-dependent answer to the question of how important these complicating factors are. Fortunately, we find that there exists a frequency regime in which the three-wave mixing polarizability does indeed reflect the local network chirality.

This is illustrated by the results of Figs. 7(a) and 7(b). Here we have computed β_a for a set of bonds in the Connell-Temkin model which have the most clearly defined chirality. These are easy to identify because in addition to having positive dihedral angles, they have a topological environment which is identical to that of a bond in polytope 240, that is, the six-membered rings passing through these bonds are arranged in the same way as they are in polytope 240. As Fig. 7(a) shows, the correlation between chirality and the sign of $\mathrm{Im}\beta_a$ is good in the high-frequency regime, that is, for frequencies beyond the peak in the oscillator strength in Fig. 6. (The frequencies used here are $\omega_1 = 11.055$ eV and $\omega_2 = -11.0$ eV.) On the other hand, the sign of β_a correlates poorly with chirality in the low-frequency regime, as Fig. 7(b) shows. (In this calculation we use $\omega_1 = 0.50$ eV and $\omega_2 = -0.49$ eV.) This poor correlation generally extends through the intermediate-frequency regime, that is, through the resonant part of the response of Fig. 6.

We have not been able to identify a simple reason for this behavior. It is tempting to speculate that the higher-energy response is more local, so that it is sensi-

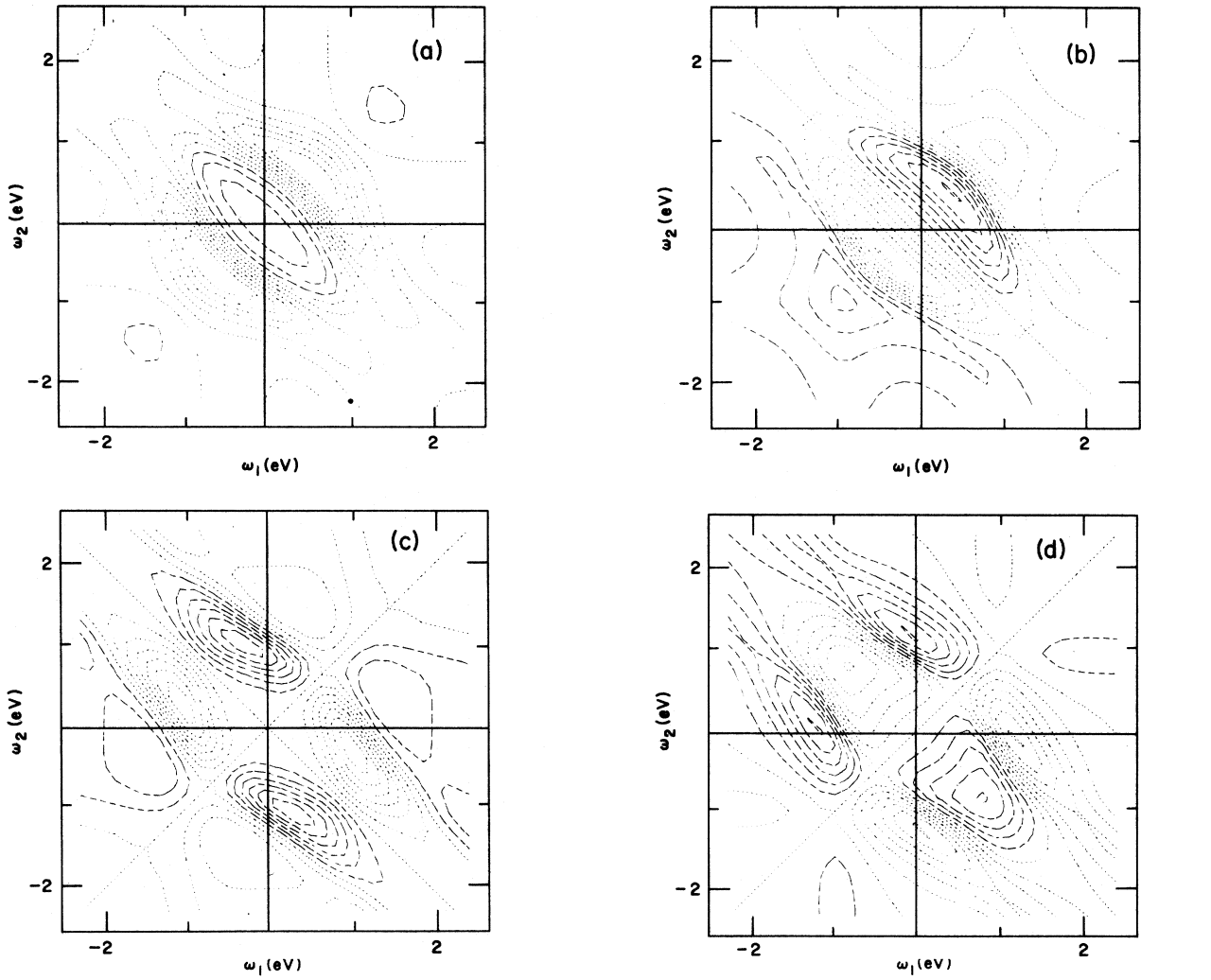

FIG. 5. The three-wave-mixing polarizability β_{123} of a two level system. (a) The real part of the symmetric response, that is, the part of β which is symmetric upon interchange of Cartesian indices. (b) The imaginary part of the symmetric response. (c) The real part of the antisymmetric response, that is, that part of β which changes sign upon interchange of Cartesian indices. As noted in the text, the antisymmetric response is relevant to probing the chirality of the network. (d) The imaginary party of the antisymmetric response. The dashed contours are positive, the dotted contours negative. The two-level system has a resonant frequency of 1 eV; this characteristic shows itself in the resonant structure of the polarizability. This and the symmetries of the different parts of the response are discussed further in the text.

tive only to the dihedral angle at that bond and not to more distant geometric or topological parameters. However, we could extract no solid evidence for this idea from our calculations. Still, taking the sensitivity of the high-frequency response to chirality as an empirical fact, we can explore its implications for three-wave-mixing experiments.

We have shown that at high frequency $\mathrm{Im}\beta_a$ is sensitive to chirality for special bonds in the network. As we now demonstrate, this property also holds for the whole random network in the Connell-Temkin model. To do this we have computed[8,48] $\langle \beta_a(\mathbf{r})\beta_a(\mathbf{r}-\mathbf{r}')\rangle$, the correlation function of the bond polarizability, averaged over $\mathbf{r}$, that is, averaged over the whole random network. This correlation function weights the contributions of all the bonds of the network equally; it is also important because, as we discuss below, it is this correlation function which directly determines the strength of the measured signal in a three-wave mixing experiment.[24]

Figure 8(a) shows the correlation function for high frequency for the two networks which we have discussed earlier: the Connell-Temkin, which we have shown to have significant chirality, and the Polk model, which has less chirality. This difference is clearly reflected in the high-frequency correlation function, which is larger and extends out to somewhat greater distance for the Connell-Temkin model than for the Polk model, reflecting both the larger average chirality and its

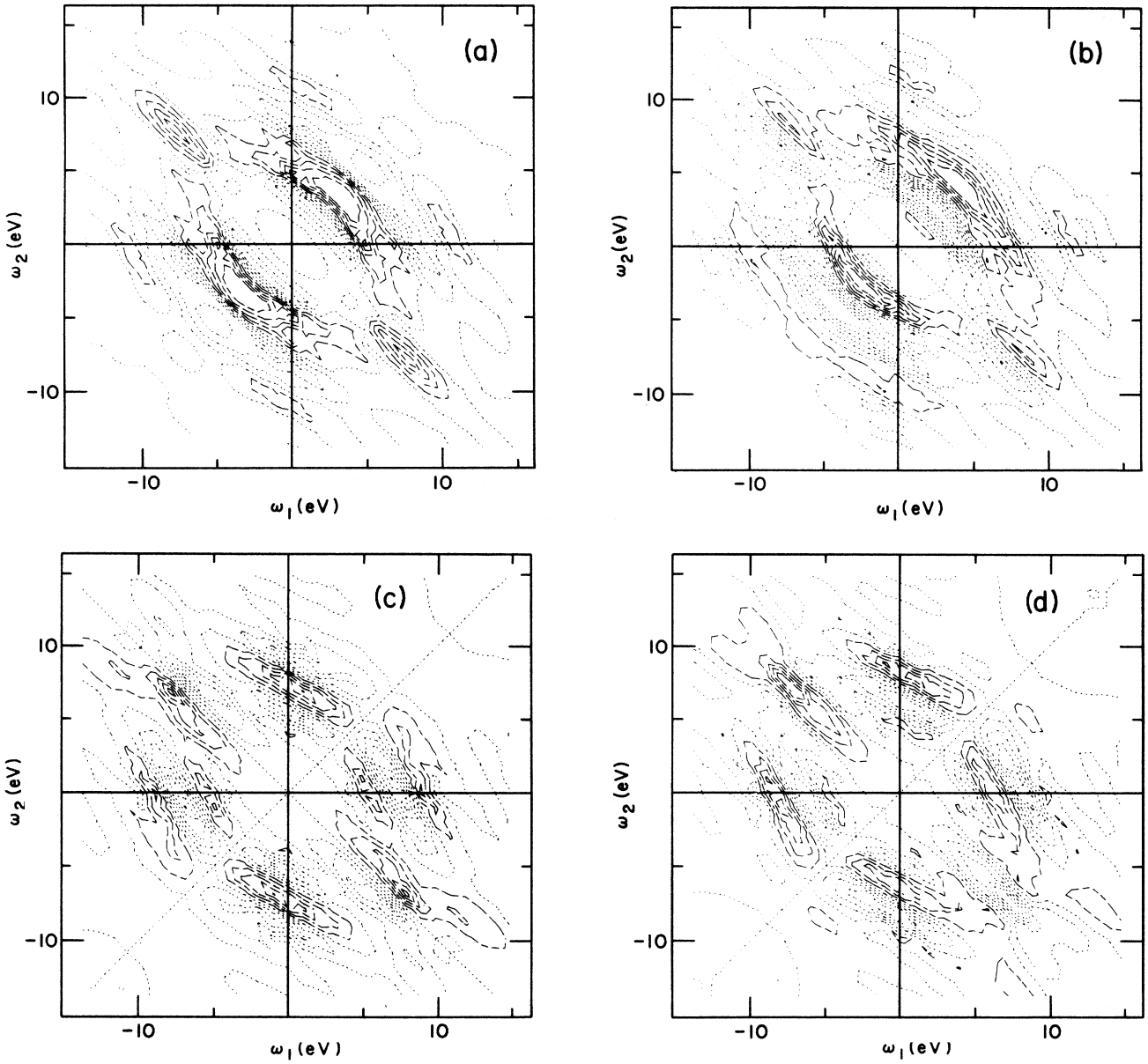

FIG. 6. The three-wave-mixing polarizability β_{123} of a typical Si—Si bond in the random network. (a) The real part of the symmetric response. (b) The imaginary part of the symmetric response. (c) The real part of the antisymmetric response. (d) The imaginary part of the antisymmetric response. The dashed contours are positive, the dotted contours negative. The maximum contour level is $0.01e^3/\mathrm{eV}^2$. Note the marked overall similarity to the response of the two-level system in Fig. 4, with the main resonance around 5 eV corresponding to the optical gap of Si.

greater spatial correlations in the Connell-Temkin model. In fact, these curves mimic closely a suitable correlation function of the ring twist discussed in the Introduction which we have published previously[8] (Fig. 9). The curves in Fig. 9 are a direct geometrical measure of the chirality in these various networks; however, the ring-twist correlation is not an experimentally measurable quantity. It is gratifying that this correlation function is closely mimicked by the polarizability correlation function, which is an *indirect* measure of chirality but *is* an experimental observable. On the other hand, the β_a correlation functions at low frequency, shown in Fig. 8(b), do not distinguish in any significant way between the Connell-Temkin and the Polk models, and thus provide a poor probe of the degree of chirality of these random networks.

We now review briefly the analysis of incoherent three-wave mixing to show how the β_a correlation function enters. The essence of the analysis is laid out carefully in a paper by Maker,[24] which considers the case of harmonic generation (i.e., $\omega_1=\omega_2$) from a disordered material; this analysis requires only the most trivial general-

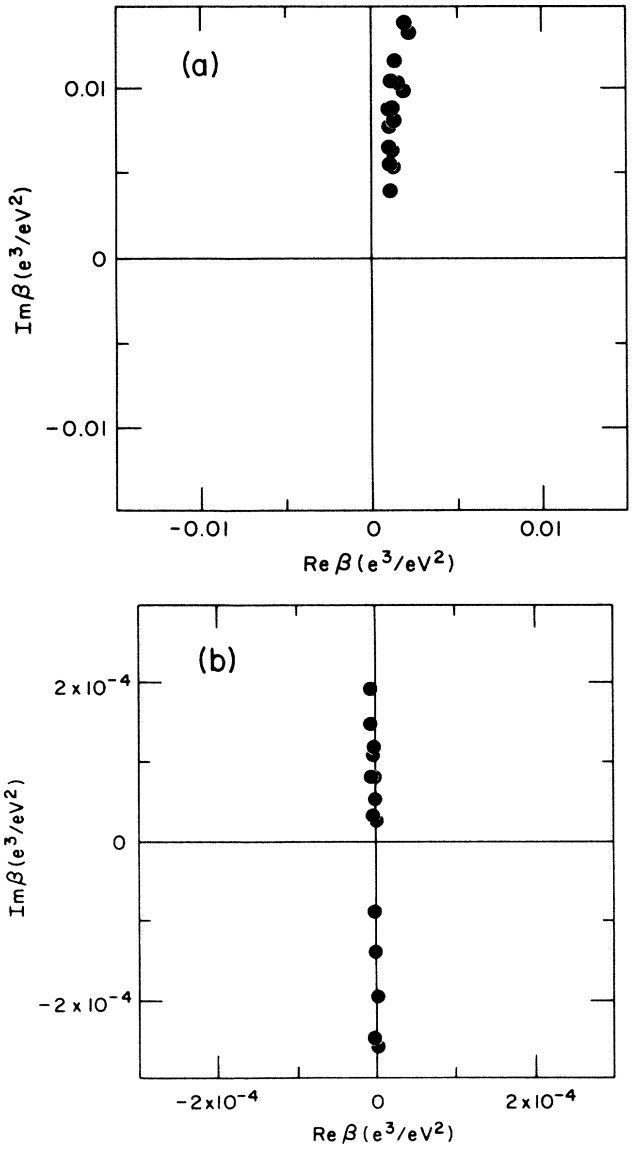

FIG. 7. The antisymmetric part of the three-wave-mixing response β_a for a set of bonds in the Connell-Temkin model, for two different choices of frequency near the inverse electro-optic limit (i.e., output frequency much less than the input frequencies). (a) $\omega_1=11.055$ eV, $\omega_2=-11.0$ eV. In this high incident frequency regime, there is an excellent correlation between the sign of Imβ_a and the chirality at the bond. (b) $\omega_1=0.50$ eV, $\omega_2=-0.49$ eV. In the low-frequency regime, the correlation between β_a and the chirality is very poor.

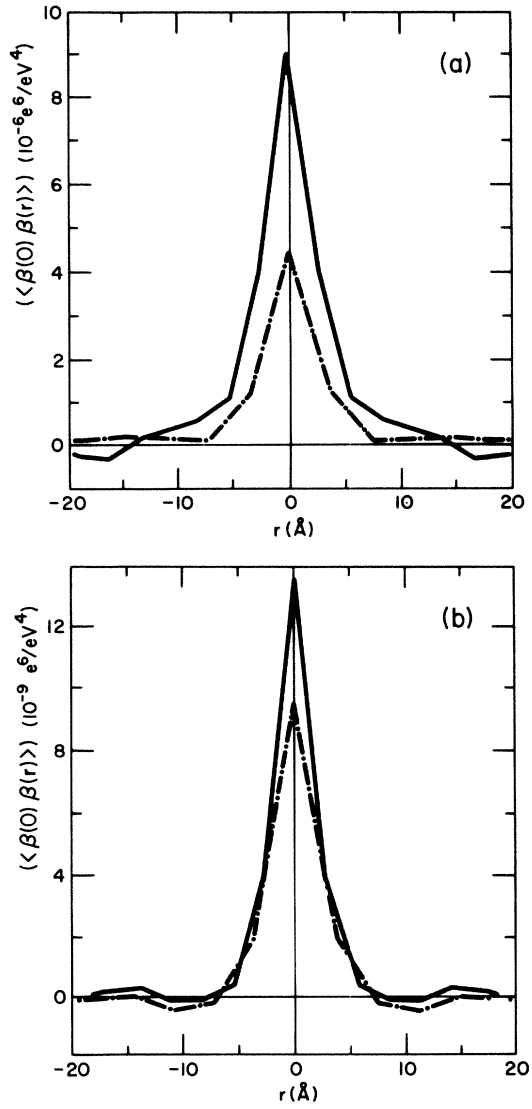

FIG. 8. The correlation function of the imaginary part of the antisymmetric three-wave-mixing polarizability, $\langle\beta_a(\mathbf{0})\beta_a(\mathbf{r})\rangle$ vs $|\mathbf{r}|$ for two different random network models, the Connell-Temkin (solid line) and the Polk (dot-dashed line). (a) High-frequency regime of Fig. 6(a). (b) Low-frequency regime of Fig. 6(b). In the first case where β_a correlates well with local chirality, the correlation function for the Connell-Temkin model is markedly larger. Recall that the Connell-Temkin model is observed to have substantial chirality, and the Polk model not. In the low-frequency regime we find the correlation function incapable of distinguishing the chiral from the nonchiral network.

ization in the present case.

We imagine the following idealized experiment: a small (say spherical, so that we can ignore Fresnel[49] factors) piece of material is illuminated with two polarized light beams, one at frequency ω_1 and the other at frequency ω_2. The material emits incoherent radiation uniformly in all directions with frequency $\omega=\omega_1+\omega_2$. The intensity of this outgoing radiation with polarization q at distance R from the sample is given by

$$I_q(R,\omega)=\frac{n}{\pi\epsilon_0 c_0^3}\left[\frac{n^2+2}{3}\right]^6\frac{1}{4\pi R^2}\omega^4 V_{\rm tot}E_\alpha(\omega_1)E_\beta(\omega_2)E_\gamma(\omega_1)E_\delta(\omega_2)\int d\mathbf{r}\langle\beta_{q\alpha\beta}(\mathbf{0})\beta_{q\gamma\delta}(\mathbf{r})\rangle\ . \tag{24}$$

This formula is very much akin to that for Rayleigh scattering,[23] and most of its factors can be identified from ordinary linear light scattering theory. The first factor contains dimensional constants (rationalized MKS units[50] are used) and the index of refraction n. c_0 is the vacuum speed of light. The second factor is a local field enhancement. The third factor simply represents the drop-off of intensity of an outgoing spherical wave. The fourth factor, the dipole radiation efficiency, is the usual Rayleigh fourth-power law. The fifth factor is the total scattering volume. The sixth factor contains the electric field strengths of the radiation at ω_1 and ω_2; α, β, γ, and δ are polarization directions.

The final factor, of course, contains all the important physics we have discussed above. Note that only the integrated strength of the polarizability correlation function affects the intensity of scattered light; higher moments of the correlation function become important only if the wavelength of the radiation becomes comparable to the correlation length, a condition which is unlikely to be achieved.

Using the numerical results obtained above we can make a rough estimate of the difficulty of the experiment being proposed. Using currently available laser technology, very large incident field strengths are achievable [$E_\alpha(\omega_{1,2})\sim 10^{10}$ V/m] in very short pulses ($\sim 10^{-13}$ sec). This field strength can only be achieved for a highly focussed beam, so the scattering volume would be rather small ($V_{\rm tot}\sim 10^{-14}$ m^3). Also, we will assume $n\sim 2$, and $\hbar\omega\sim 0.1$ eV. From Fig. 8(a), the integrand polarizability is about $10^{-4}e^3$ Å^3/eV^2 for the Connell-Temkin model, and perhaps a factor of 2 smaller for the Polk model. With these numbers, the instantaneous power, integrated over all 4π of solid angle, is about 10^{-4} W, which is about 10^3 infrared photons per 100 fs pulse. For a pulse repetition rate of 10^8 Hz, this translates into an average power of about 100 pW. While this is not an overwhelmingly large signal, it is in a detectable range. To distinguish "Connell-Temkin-like" from "Polk-like" networks, one would need to measure the absolute intensity [Eq. (24)] to an accuracy of about a factor of 2 [i.e., the difference in the integrated correlation functions of Fig. 8(a)].

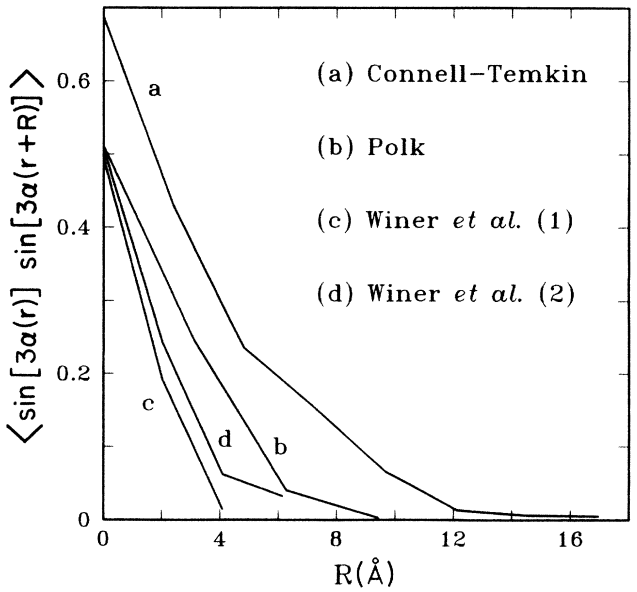

FIG. 9. A correlation function for ring twist computed numerically for four different random network models for amorphous semiconductors. Details of this calculation are given elsewhere (Ref. 8). This calculation provides a direct measure of the geometric chirality in the network; the Connell-Temkin model is the most chiral among the ones studied. The "Winer models" (Ref. 22) are the least chiral.

Unfortunately, this treatment glosses over a significant background signal which comes from the uninteresting "symmetric" part of the three-wave mixing response. Contributions to Eq. (24) come from the *total* polarizability tensor β_{ijk}, not just from those parts with a particular symmetry with respect to interchange of tensor indices.[51,52] This problem can be largely solved by combining the results of the experiment done under different polarization conditions. We shall not delve into this analysis in detail, since the actual experimental polarizations will certainly depend on various considerations of practical convenience. We find, however, that one procedure which will work in principle is to combine the results of the following two experiments. (1) Send in light at frequency ω_1 with linear polarization in the x direction, and light at frequency ω_2 with linear polarization in the y direction; detect the scattered light polarized in the z direction; call the resulting intensity $\mathbf{I}^1$. (2) Send in left circularly polarized light at ω_1, and right circularly polarized light at ω_2 (both in the x-y plane); again detect the emitted light with z polarization, calling the result $\mathbf{I}^2$. The quantity $2\mathbf{I}^1-\mathbf{I}^2$ has no contributions from the symmetric part of the polarizability, containing only antisymmetry contributions; that is, the ones which are chirality sensitive. (Actually, this quantity is still not perfect, because it contains some partly antisymmetric parts along with the fully antisymmetric part. We can show that this is not a serious problem, because these additional unwanted contributions are fairly small.)

The reader may worry that $2\mathbf{I}^1$, $\mathbf{I}^2 \gg 2\mathbf{I}^1 - \mathbf{I}^2$, that is, the symmetric response will overwhelm the antisymmetric response which is of interest to us. Our calculations of the symmetric response, which we have not reported, show that these concerns are not serious, because we find that the symmetric and antisymmetric responses are comparable in magnitude in the high-frequency regime of interest. This is by contrast to the low-frequency regime, where most practical experience has been gained and on which most intuition is founded,[24,28] in which the symmetric response is dominant.

IV. CONCLUSIONS

Our hope is that the study of incoherent three-wave mixing in disordered materials goes beyond the specific proposals of the present paper. Already, other workers have used *four*-wave mixing (i.e., third-harmonic generation) to gain information about the amorphization transition in ion-bombarded Si.[53,54] However, there seems to have been a disinclination to try *three*-wave mixing in the past,[55] possibly because disordered materials are macroscopically isotropic, which might be expected to make the three-wave mixing response vanish. What has perhaps not been previously appreciated is that while disordered solids are isotropic on a *macroscopic* scale, they are not on a *microscopic* scale, so that while *coherent* three-wave mixing is forbidden, *incoherent* three-wave mixing is not, and should in fact be quite informative about the microscopic structure of the solid.

Other materials besides amorphous Si and Ge should certainly be amenable to the kind of study proposed here.[55] For example, in the common network glasses (e.g., SiO_2) similar questions can be asked about the intermediate-range chirality of the network structure. Such chirality would actually be less surprising in SiO_2 than in Si, since chiral crystalline forms of silica are well known (e.g., quartz). A theoretical study of the three-wave mixing response in this system would focus on the polarizability of the Si—O—Si unit and how it is influenced by the dihedral angles of the neighboring oxygens.

A very different example is provided by the amorphous III-V materials. Here the physics of the three-wave mixing is different, because even crystalline, nonchiral III-V solids have a large three-wave mixing response because of the asymmetry of the bonds[34] in the material. Thus we would expect the antisymmetric (i.e., chiral) part of the response in the amorphous material to be swamped by the strong nonchiral bond response. Still, this response can be put to good use; measurement of the three-wave mixing in these materials should give a measure of the bond-orientation correlation function, a quantity not easily accessible to other experiments.

In summary, we have considered the question of how local network chirality (defined, for example, by the sign of the dihedral angle) can be experimentally probed in amorphous semiconductors. A definite local chirality is an important feature of recent polytope models of amorphous semiconductors, and local chirality can be identified in at least one hand-built continuous random network, the Connell-Temkin model; yet, no previous direct experimental test has been proposed. On the basis of symmetry arguments, we show that the local three-wave mixing response is a good candidate for probing this chirality, at least in the "inverse electro-optic" limit where two of the waves have nearly equal frequency and the difference frequency response at low frequency is measured. We work out the formalism for properly computing this local response in the tight-binding approximation. We find that in the high-incident-frequency regime, the local polarizability does indeed follow the local chirality. The effects of this local chirality should be detectable in a real scattering experiment.

ACKNOWLEDGMENTS

I thank E. J. Mele, D. C. Allan, and J. Tersoff for helpful discussions of tight-binding polarizabilities, O. L. Alerhand for providing his tight-binding programs, J. Tsang and J. Kash for general education about fast laser experiments, A. Heinz and E. Burstein for most of what I know about the phenomenology of harmonic generation and three-wave mixing, R. Mosseri and J.-F. Sadoc for much enlightenment about the properties of polytopes, and M. H. Brodsky for his great knowledge and continuing interest in amorphous Si and unconventional models thereof.

APPENDIX

1. Ring twist and symmetry

The symmetry properties of the various configurations of six-membered rings determine how much structural freedom they have, i.e., they determine whether or not the six-membered rings are "nonrigid." An isolated "chair" ring has threefold rotation symmetry as well as mirror reflection symmetries; its point group is $\bar{3}m$ (D_{3d}). A boat ring has twofold symmetry and two mirror symmetries, with a point-group symmetry of $mm2$ (C_{2v}). The "twisted boat" loses the mirror reflections, retaining only the twofold rotational symmetry (point group 2, or C_2). We now show that a six-membered ring with a twofold symmetry has a continuous one-parameter family of twists. The essence of this is a constraint-counting argument, which goes as follows. The six vertices of the ring in three dimensions initially have $6\times 3 = 18$ degrees of freedom. This is immediately reduced by half by the twofold symmetry, leaving nine. Among these, one is a trivial translational degree of freedom along the twofold axis, and one a trivial rotation about it; removing these leaves seven degrees of freedom. Then there are six bond angle and six bond length constraints, only half of which are distinct because of the symmetry. Subtracting these away leaves one degree of freedom, which corresponds to the nontrivial twist variable mentioned above. When a similar counting argument is constructed for a subgroup of the "chair" symmetry (e.g., just threefold symmetry), no degrees of free-

dom are left; and indeed, the "chair" ring is rigid against infinitesimal distortions.

2. Single-particle expression for three-wave mixing susceptibility

Here we discuss the complete transcription of the many-body formula for the polarizability [Eq. (5)] for the case of a noninteracting Fermi sea.[56] We present this here because, so far as we can tell, a correct formula of this sort has not previously been presented in the literature. In the interests of economy we will invent a diagrammatic notation from which the complete 16-term expression may be reconstructed. These diagrams should not be confused with the diagrams used in Green's-function theories of polarizabilities; while they represent the same calculation, they organize the algebra in different ways.

The diagrams are shown in Fig. 10. Their form may be interpreted in a suggestive way: The first photon interacts with the solid, creating an electron-hole pair. Then the second photon scatters one of these two lines. Finally, the two lines annihilate, emitting a photon at the sum frequency. While this picture is useful, the diagrams should really only be used as rules for generating the correct algebraic expression for the three-wave-mixing tensor. These rules are as follows.

(1) Associate single-particle state labels with each of the fermion lines (α, β, and γ in Fig. 11).

(2) Incident photons are denoted by wavy lines. Associate one of the two incident frequencies with the first photon line (ω_2 in Fig. 11), and the other with the second photon line (ω_1 in Fig. 11). $\omega=\omega_1+\omega_2$ is always the frequency of the outgoing line. Each diagram generates two terms corresponding to the two different assignments of the incident frequencies.

(3) Each vertex has a dipole matrix element associated with it. In particular, the ω vertex is associated with the dipole operator $\hat{r}_i^{\text{bond}}$, the ω_1 vertex with $\hat{r}_j$, and the ω_2 vertex with $\hat{r}_k$. Thus the diagram in Fig. 11 generates the factors $\langle\gamma|\hat{r}_k|\alpha\rangle$, $\langle\gamma|\hat{r}_j|\beta\rangle$, and $\langle\beta|\hat{r}_i^{\text{bond}}|\alpha\rangle$.

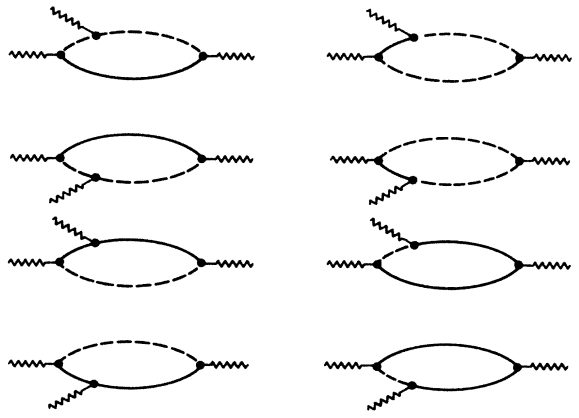

FIG. 10. The eight distinct diagrams which can be used to generate the one-particle expression for the three-wave-mixing polarizability. Solid lines denote holes, dashed lines electrons, and wavy lines photons coming in or out. Detailed rules are given in the Appendix.

(Since we take the system to be finite, the states are real and we do not distinguish the matrix element from its adjoint.)

(4) Solid lines denote holes; thus, they are associated with a fermi factor. (f_a in Fig. 11.) Dashed lines denote electrons ($1-f_\beta$ and $1-f_\gamma$ in Fig. 11).

(5) The double Fermion lines which go from one vertex to the next are associated with the propagator factor

$$\frac{1}{\sum_{i(\text{left})}\omega_i-(\omega_{\text{upper}}-\omega_{\text{lower}})+i\Gamma_{\text{upper,lower}}}\ . \tag{A1}$$

Here the sum runs over the frequencies associated with the vertices to the left, ω_{upper} is the eigenenergy of the state associated with the upper fermion line, ω_{lower} is the corresponding energy for the lower fermion line, and $\Gamma_{\text{upper,lower}}$ is the damping constant for transitions between these states. The two denominator factors so generated are shown in Fig. 11.

(6) There is a nontrivial overall signal which is associated with the antisymmetry of the total wave function.[39] The rule for the sign is, if an electron line enters the second vertex from the left, the sign is positive; if it is a hole line, the overall sign is negative.

(7) Finally, there is an overall factor $e^3/V^{\text{bond}}\hbar^2$.

The eight diagrams in Fig. 10 generate 16 distinct terms, since there are two ways that the two incident frequencies can be assigned to the first pair of vertices.

3. Current form of three-wave mixing polarizability

It is possible to derive an alternative form for the three-wave mixing polarizability in which current operators rather than dipole operators appear in expressions like Eqs. (5) and (13). This will be desirable when the system of interest is a crystal rather than a cluster. Here we will discuss the construction of this expression within the one-particle approximation only. We will see that this expression is a great deal more complicated, particularly in the tight-binding approximation. This, as well as the delicacy of the zero-frequency limit in this representation, discouraged us from actually using this form. In this appendix we consider only the $\lambda\to\infty$ limit, where λ

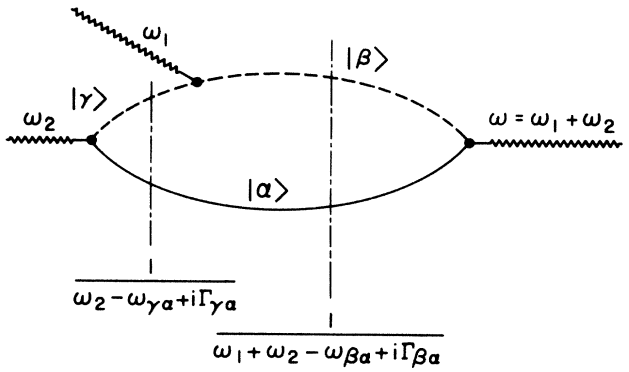

FIG. 11. Detailed labeling of a diagram. Each line is associated with a single-particle state label α, β, and γ, each photon line is associated with a frequency label, and each pair of fermion lines is associated with the denominator factor indicated.

is the light wavelength.

Using the current form rather than the dipole form of the text means two things: (1) changing the gauge so that the electric field enters the Hamiltonian through the vector potential rather than the scalar potential, and (2) considering as the measurable quantity the local current density $\mathbf{J}(\mathbf{r})$ rather than the polarization density $\mathbf{P}(\mathbf{r})$. The two are related as in Eq. (12).

The vector potential which is equivalent to the scalar potential in Eq. (4) is

$$\mathbf{A}(\mathbf{R},t)=\frac{ic\mathbf{E}_1 e^{i\omega_1 t}}{\omega_1}+\frac{ic\mathbf{E}_2 e^{i\omega_2 t}}{\omega_2} . \tag{A2}$$

Specializing to the tight-binding problem, we ask the question, how do we perform the gauge transformation which makes the scalar potential zero, putting all the field into the vector potential? In tight-binding language, this is the same as finding the (time-dependent) unitary transformation which will remove the scalar potential from the time-dependent tight-binding Schrödinger equation:

$$[h_{\alpha\beta}+\delta_{\alpha\beta}\phi(R_\alpha,t)]\psi_\beta=\frac{\hbar}{i}\frac{\partial}{\partial t}\psi_\alpha . \tag{A3}$$

It is easy to verify that the required unitary transformation is

$$U_{\alpha\beta}=\delta_{\alpha\beta}e^{-i(e/\hbar c)\mathbf{R}_\alpha\cdot\mathbf{A}(t)} , \tag{A4}$$

with $\mathbf{A}(t)$ given in Eq. (A2). Here $\mathbf{R}_\alpha$ is the position vector of orbital α [see Eqs. (17) and (18) in the text]. The new Schrödinger equation is

$$\tilde{h}_{\alpha\beta}\psi_\beta=\frac{\hbar}{i}\frac{\partial}{\partial t}\psi_\alpha , \tag{A5}$$

where the modified Hamiltonian is

$$\tilde{h}_{\alpha\beta}=h_{\alpha\beta}e^{-i(e/\hbar c)(\mathbf{R}_\alpha-\mathbf{R}_\beta)\cdot\mathbf{A}} . \tag{A6}$$

It is widely[57,58] but not universally known in the tight-binding literature that Eq. (A6) is the uniquely correct way to introduce the vector potential in a gauge-invariant fashion.

We need to compute the response of the system to second order in the applied electric fields; expanding Eq. (A6) in powers of $\mathbf{A}$ and substituting in Eq. (A2) gives

$$\delta\tilde{h}_{\alpha\beta}=\left[\frac{e}{\hbar\omega_1}h_{\alpha\beta}\mathbf{R}_{\alpha\beta}\cdot\mathbf{E}_1 e^{i\omega_1 t}+\frac{e}{\hbar\omega_2}h_{\alpha\beta}\mathbf{R}_{\alpha\beta}\cdot\mathbf{E}_2 e^{i\omega_2 t}\right]+\frac{e^2}{\hbar^2\omega_1\omega_2}h_{\alpha\beta}\mathbf{R}_{\alpha\beta}\cdot\mathbf{E}_1\mathbf{R}_{\alpha\beta}\cdot\mathbf{E}_2 e^{i(\omega_1+\omega_2)t}+\cdots+O(E^3)+\cdots$$
$$=\delta h^{(1)}_{\alpha\beta}+\delta h^{(2)}_{\alpha\beta}+\delta h^{(3)}_{\alpha\beta}+\cdots . \tag{A7}$$

Here $\mathbf{R}_{\alpha\beta}\equiv\mathbf{R}_\alpha-\mathbf{R}_\beta$.

Note that this expression contains not only pieces which are of first and second order in the applied fields, but all higher orders as well. This is peculiar to tight binding (i.e., finite Hilbert space) calculations; it should be contrasted with the case of ordinary quantum mechanics, where the perturbation Hamiltonian in this gauge is

$$\delta h=-\frac{e}{mc}(\mathbf{p}\cdot\mathbf{A})+\frac{e^2}{2mc^2}A^2 . \tag{A8}$$

Here there are rigorously no contributions to the Hamiltonian beyond second order in the applied field. Moreover, the A^2 term is an identity operator in the electron space (because our vector potential has no spatial dependence), which means that this term cannot cause transitions, therefore contributing nothing to the polarizability. In a tight-binding theory the second-order term (as well as all higher-order terms) can cause transitions, contributes to the susceptibility, and complicates the calculation considerably.

Additional major complications arise from computing the expectation value of the bond current $\hat{\mathbf{J}}^{\text{bond}}/i(\omega_i+\omega_2)$ rather than the bond dipole $e\hat{\mathbf{R}}^{\text{bond}}$ [remember Eq. (12)]. The one-particle matrix elements of the current density operator are given by

$$\mathbf{J}_{\alpha\beta}(\mathbf{R})=\frac{e}{2}\sum_\gamma[\mathbf{v}_{\alpha\gamma}\phi^*_\gamma(\mathbf{R})\phi_\beta(\mathbf{R})+\phi^*_\alpha(\mathbf{R})\phi_\gamma(\mathbf{R})\mathbf{v}_{\gamma\beta}] . \tag{A9}$$

Here $\phi_\alpha(\mathbf{R})$ is the basis function introduced in Eq. (16), using a slightly different notation. $\mathbf{v}$ is the electron velocity operator $\dot{\mathbf{R}}$, which is conveniently evaluated using the Heisenberg equation of motion:

$$\mathbf{v}_{\alpha\beta}=\dot{\mathbf{R}}_{\alpha\beta}=\frac{1}{i\hbar}[\mathbf{R},\tilde{h}]_{\alpha\beta} . \tag{A10}$$

$\tilde{h}$ is the *full* Hamiltonian including the radiation field [Eq. (A6)]. Using the diagonal form given in Eq. (17) for the operator $\hat{\mathbf{R}}$, we can evaluate the commutator:

$$\mathbf{v}_{\alpha\beta}=\frac{1}{i\hbar}\mathbf{R}_{\alpha\beta}\tilde{h}_{\alpha\beta} . \tag{A11}$$

Now we actually want the bond current,

$$\hat{\mathbf{J}}^{\text{bond}}=\int_{\text{bond}}\hat{\mathbf{J}}(\mathbf{R})d\mathbf{R} . \tag{A12}$$

Putting this together, we get

$$J_{\alpha\beta}^{\text{bond}}=\frac{e}{2i\hbar}\sum_{\gamma}(e^{-i(e/\hbar c)\mathbf{R}_{\alpha\gamma}\cdot\mathbf{A}}\mathbf{R}_{\alpha\gamma}h_{\alpha\gamma}\theta_{\gamma\beta}^{\text{bond}} +\theta_{\alpha\gamma}^{\text{bond}}e^{-i(e/\hbar c)\mathbf{R}_{\gamma\beta}\cdot\mathbf{A}}\mathbf{R}_{\gamma\beta}h_{\gamma\beta}) . \tag{A13}$$

θ^{bond} is defined in Eq. (20). Now, like the Hamiltonian, the current operator can be expanded in a power series in the vector potential:

$$J_{\alpha\beta}^{\text{bond}}=\frac{e}{2i\hbar}\sum_{n=0}^{\infty}\sum_{\gamma}\left[\mathbf{R}_{\alpha\gamma}h_{\alpha\gamma}\theta_{\gamma\beta}^{\text{bond}}\frac{1}{n!}\left[-\frac{ie}{\hbar c}\right]^{n}(\mathbf{R}_{\alpha\gamma}\cdot\mathbf{A})^{n}+\theta_{\alpha\gamma}^{\text{bond}}\mathbf{R}_{\gamma\beta}h_{\gamma\beta}\frac{1}{n!}\left[-\frac{ie}{\hbar c}\right]^{n}(\mathbf{R}_{\gamma\beta}\cdot\mathbf{A})^{n}\right]$$
$$=\sum_{n}J_{\alpha\beta}^{\text{bond}(n)} . \tag{A14}$$

Comparing Eq. (A7) and Eq. (A14), we find a relationship between the terms in the expansion of the current operator and those of the perturbation Hamiltonian:

$$\frac{e}{(n+1)c}\mathbf{J}_{\alpha\beta}^{\text{bond}(n)}\cdot\mathbf{A} =-\frac{1}{2}\sum_{\gamma}(\delta h_{\alpha\gamma}^{(n+1)}\theta_{\gamma\beta}^{\text{bond}}+\theta_{\alpha\gamma}^{\text{bond}}\delta h_{\gamma\beta}^{(n+1)}) . \tag{A15}$$

It is interesting to note that for the case of the total current operator rather than the bond current operator, this relation simplifies to

$$\frac{e}{(n+1)c}\hat{\mathbf{J}}^{(n)}\cdot\mathbf{A}=-\delta\hat{h}^{(n+1)} . \tag{A16}$$

This relation, while derived within tight binding, is rigorously true in quantum mechanics, in which the various terms are

$$\hat{\mathbf{J}}^{(0)}=\frac{\hat{\mathbf{p}}}{m},\quad \delta\hat{h}^{(1)}=-\frac{e}{mc}\hat{\mathbf{p}}\cdot\mathbf{A} ,$$
$$\hat{\mathbf{J}}^{(1)}=-\frac{e\mathbf{A}}{mc}\hat{1},\quad \delta\hat{h}^{(2)}=\frac{e^{2}}{2mc^{2}}A^{2}\hat{1} , \tag{A17}$$
$$\hat{\mathbf{J}}^{(n)}=0,\quad \delta\hat{h}^{(n+1)}=0,\quad n>1 .$$

$\hat{1}$ is the identity operator in the electron space. The main difference and complication of tight binding is that these terms do not vanish for any $n>1$.

It should be noted that the above derivation relied on the assumption that the matrix elements of the position operator are diagonal in the tight-binding orbital representation [i.e., Eq. (17)]. In previous work it has been considered physically sensible to add on-site off-diagonal "atomiclike" matrix elements,[42] corresponding, for example, to s to p transitions:

$$\langle i,s\mid r_{x}\mid i,p_{x}\rangle\neq 0 . \tag{A18}$$

Introducing this kind of matrix element invalidates Eq. (18), and more importantly, violates another important rigorous equation of quantum mechanics $[r_x,r_y]=0$. Thus the introduction of these additional terms in the dipole matrix, while apparently well-motivated physically, is not advisable on formal grounds.

With all this background, we return to the issue of the construction of the three-wave mixing polarizability within the current (as opposed to dipole) formulation. It is an exercise in perturbation theory; in outline, one proceeds as follows.

The response of the system, the expectation value of the bond polarization, is computed using the density matrix [see also Eq. (12)]:

$$\langle\hat{\mathbf{P}}^{\text{bond}}\rangle^{(2)}=\frac{1}{i(\omega_1+\omega_2+i\Gamma)}\langle\hat{\mathbf{J}}^{\text{bond}}\rangle^{(2)}$$
$$=\frac{1}{i(\omega_1+\omega_2+i\Gamma)}[\mathrm{Tr}(\hat{\rho}^{(2)}\hat{\mathbf{J}}^{\text{bond}(0)}) +\mathrm{Tr}(\hat{\rho}^{(1)}\hat{\mathbf{J}}^{\text{bond}(1)}) +\mathrm{Tr}(\hat{\rho}^{(0)}\hat{\mathbf{J}}^{\text{bond}(2)})] . \tag{A19}$$

We have inserted the damping factor Γ following Mermin.[59] The superscripts in this equation denote the order to which the electric field appears. Recall that the third term is special to tight binding. Each of these three terms will lead to distinct sets of contributions to the three-wave mixing susceptibility. We consider each of these in turn.

a. $Tr(\hat{\rho}^{(2)}\hat{J}^{\text{bond}(0)})$ term

To evaluate the density matrix, we use the Heisenberg equation of motion:

$$\frac{\partial\hat{\rho}^{(2)}}{\partial t}=i(\omega_1+\omega_2+i\Gamma)\hat{\rho}^{(2)}=\frac{1}{i\hbar}[\tilde{h},\hat{\rho}]^{(2)}$$
$$=\frac{1}{i\hbar}([h^{(0)},\hat{\rho}^{(2)}]+[\delta h^{(1)},\hat{\rho}^{(1)}]+[\delta h^{(2)},\hat{\rho}^{(0)}])\ . \tag{A20}$$

Taking matrix elements between eigenstates α and β gives

$$i(\omega_1+\omega_2-\omega_{\alpha\beta}+i\Gamma)\hat{\rho}^{(2)}_{\alpha\beta}$$
$$=\frac{1}{i\hbar}([\delta h^{(1)},\hat{\rho}^{(1)}]_{\alpha\beta}+[\delta h^{(2)},\hat{\rho}^{(0)}]_{\alpha\beta})\ . \tag{A21}$$

The two terms on the right-hand side of Eq. (A21) in turn generate distinct sets of contributions to the polarizability.

(1) The first commutator generates 16 terms which are exactly parallel to the 16 terms of the polarizability in the dipole form. One set can be obtained from the other by the following replacement:

$$(\hat{r}_i^{\,\mathrm{bond}})_{\alpha\beta}\Longleftarrow\frac{\sum_\gamma[(R_i)_{\alpha\gamma}h_{\alpha\gamma}\theta^{\mathrm{bond}}_{\gamma\beta}+\theta^{\mathrm{bond}}_{\alpha\gamma}(R_i)_{\gamma\beta}h_{\gamma\beta}]}{2\hbar(\omega_1+\omega_2+i\Gamma)}\ ,$$
$$(\hat{r}_j)_{\alpha\beta}\Longleftarrow\frac{(R_j)_{\alpha\beta}h_{\alpha\beta}}{\hbar(\omega_1+i\Gamma)}\ , \tag{A22}$$
$$(\hat{r}_k)_{\alpha\beta}\Longleftarrow\frac{(R_k)_{\alpha\beta}h_{\alpha\beta}}{\hbar(\omega_2+i\Gamma)}\ .$$

(2) The second commutator generates two terms which have the same structure as the linear susceptibility:[28]

$$\frac{e^3}{\hbar V^{\mathrm{bond}}}\sum_{\alpha,\beta}(1-f_\alpha)f_\beta\left[\frac{(\hat{\Xi}_1)_{\alpha\beta}(\hat{\Xi}_2)_{\beta\alpha}}{\omega+\omega_{\alpha\beta}+i\Gamma_{\alpha\beta}}-\frac{(\hat{\Xi}_2)_{\alpha\beta}(\hat{\Xi}_1)_{\beta\alpha}}{\omega-\omega_{\alpha\beta}+i\Gamma_{\alpha\beta}}\right]\ . \tag{A23}$$

The matrix elements of the operators $\hat{\Xi}_1$ and $\hat{\Xi}_2$ are

$$(\hat{\Xi}_1)_{\alpha\beta}\Longleftarrow\frac{\sum_\gamma[(R_i)_{\alpha\gamma}h_{\alpha\gamma}\theta^{\mathrm{bond}}_{\gamma\beta}+\theta^{\mathrm{bond}}_{\alpha\gamma}(R_i)_{\gamma\beta}h_{\gamma\beta}]}{2\hbar(\omega_1+\omega_2+i\Gamma)}\ ,$$
$$(\hat{\Xi}_2)_{\alpha\beta}\Longleftarrow\frac{h_{\alpha\beta}(R_j)_{\alpha\beta}(R_k)_{\alpha\beta}}{\hbar^2(\omega_1+i\Gamma)(\omega_2+i\Gamma)}\ . \tag{A24}$$

Equation (A23) does not appear in a rigorous treatment of the three-wave mixing, because in exact quantum mechanics $\hat{\Xi}_2$ has only diagonal matrix elements; this is not true in the tight-binding approximation, however.

b. $Tr(\hat{\rho}^{(1)}\hat{J}^{\mathrm{bond}\ (1)})$ term

The equation analogous to Eq. (A21) for this term is

$$i(\omega_\mu-\omega_{\alpha\beta}-i\Gamma)\hat{\rho}^{(1)}_{\alpha\beta}=\frac{1}{i\hbar}[\delta h^{(1)},\hat{\rho}^{(0)}]_{\alpha\beta}\ . \tag{A25}$$

Here ω_μ is either ω_1 or ω_2. $\hat{\mathbf{J}}^{\mathrm{bond}\ (1)}$ also contains either the frequency factor ω_1 or ω_2, which we will denote ω_ν; it is required that $\mu\neq\nu$. From this we again generate two terms which are identical in form to Eq. (A23) with the identifications

$$(\hat{\Xi}_1)_{\alpha\beta}\Longleftarrow\frac{\sum_\gamma[(R_i)_{\alpha\gamma}(R_\xi)_{\alpha\gamma}h_{\alpha\gamma}\theta^{\mathrm{bond}}_{\gamma\beta}+\theta^{\mathrm{bond}}_{\alpha\gamma}h_{\gamma\beta}(R_i)_{\gamma\beta}(R_\xi)_{\gamma\beta}]}{2\hbar^2(\omega_1+\omega_2+i\Gamma)(\omega_\nu+i\Gamma)}\ ,$$
$$(\hat{\Xi}_2)_{\alpha\beta}\Longleftarrow\frac{(R_\xi)_{\alpha\beta}h_{\alpha\beta}}{\hbar(\omega_\mu+i\Gamma)}\ . \tag{A26}$$

The Cartesian indices ξ and ζ are determined by the frequency labels μ and ν. If $\mu=1$ and $\nu=2$, then $\xi=k$ and $\zeta=j$, and vice versa. Because of these two possibilities, four distinct terms are generated. These terms also occur in rigorous quantum mechanics; they are the higher-order analogue of the "diagmagnetic"[39] contributions to the polarizability in the linear case.

c. $Tr(\hat{\rho}^{(0)}\hat{J}^{\mathrm{bond}\ (2)})$ term

This may be simply evaluated, giving a single term:

$$\frac{-e^3\sum_{\alpha\gamma}f_\alpha[(R_i)_{\alpha\gamma}(R_j)_{\alpha\gamma}(R_k)_{\alpha\gamma}h_{\alpha\gamma}\theta^{\mathrm{bond}}_{\gamma\alpha}+\theta^{\mathrm{bond}}_{\alpha\gamma}h_{\gamma\alpha}(R_i)_{\gamma\alpha}(R_j)_{\gamma\alpha}(R_k)_{\gamma\alpha}]}{2\hbar^3V^{\mathrm{bond}}(\omega_1+\omega_2+i\Gamma)(\omega_1+i\Gamma)(\omega_2+i\Gamma)}\ . \tag{A27}$$

This term does not occur in exact quantum mechanics, where $\hat{J}^{\mathrm{bond}\ (2)}=0$.

This completes our derivation of the current form of the three-wave mixing susceptibility—23 terms in all, a very cumbersome tool indeed. Of course, it is possible to construct a mixed formalism in which both current and dipole operators appear; we shall not discuss this here.

One might think that it would be sensible to approximate the polarizability by throwing away some of the 23 terms, at least the ones which are zero in rigorous quantum mechanics, in order to make the calculation somewhat more manageable. This would be very unwise, for the following reason. All of the individual terms in the polarizability diverge at zero frequency; however, the total polarizability must in fact be finite at zero frequency. This means that there is a delicate cancellation among all of these 23 terms; leaving a few of them out leads to nonsensical answers at low frequency.

[1]M. Kleman and J. F. Sadoc, J. Phys. (Paris) Lett. **40**, L569 (1979).

[2]J. F. Sadoc, J. Non-Cryst. Solids **44**, 1 (1981).

[3]H. S. M. Coxeter, *Regular Polytopes* (Meuthen, London, 1948).

[4]D. R. Nelson, Phys. Rev. B **28**, 5515 (1983).

[5]J. F. Sadoc, J. Phys. (Paris) Lett. **44**, L707 (1983).

[6]D. R. Nelson, Phys. Rev. Lett. **50**, 982 (1983).

[7]R. Mosseri, D. P. DiVincenzo, J. F. Sadoc, and M. H. Brodsky, Phys. Rev. B **32**, 3974 (1985).

[8]D. P. DiVincenzo and M. H. Brodsky, J. Non-Cryst. Solids **77&78**, 241 (1985).

[9]H. S. M. Coxeter, *Regular Complex Polytopes* (Cambridge University Press, London, 1974).

[10]Patrick DuVal, *Homographies, Quaternions, and Rotations* (Clarendon, Oxford, 1964).

[11]Subir Sachdev and David R. Nelson, Phys. Rev. Lett. **53**, 1947 (1984).

[12]Subir Sachdev, Phys. Rev. B **33**, 6395 (1986).

[13]J. F. Sadoc and R. Mosseri, Philos. Mag. B **45**, 467 (1982).

[14]Actually an old one: G. de B. Robinson, Proc. Cambridge Philos. Soc. **27**, 37 (1931); H. S. M. Coxeter, Philos. Trans. R. Soc. London, Ser. A **229**, 346 (1930).

[15]J. F. Sadoc and R. Mosseri, J. Phys. (Paris) Colloq. **42**, C4-189 (1981).

[16]V. Elser (unpublished).

[17]Dihedral angle disorder in amorphous networks has been studied previously by J. Singh, Phys. Rev. B **23**, 4156 (1981).

[18]S. Sachdev and D. R. Nelson (unpublished).

[19]G. A. N. Connell and R. J. Temkin, Phys. Rev. B **9**, 5323 (1974).

[20]D. E. Polk and D. S. Boudreaux, Phys. Rev. Lett. **31**, 92 (1973).

[21]P. J. Steinhardt, R. Alben, and D. Weaire, J. Non-Cryst. Solids **15**, 199 (1974).

[22]F. Wooten, K. Winer, and D. Weaire, Phys. Rev. Lett. **54**, 1392 (1985); K. Winer, Phys. Rev. B **35**, 2366 (1987).

[23]M. Cardona, *Light Scattering in Solids II: Basic Concepts and Instrumentation,* edited by M. Cardona and G. Güntherodt (Springer, Berlin, 1982), p. 22ff.

[24]P. D. Maker, Phys. Rev. A **1**, 923 (1970).

[25]R. Alben, D. Weaire, J. E. Smith, Jr., and M. H. Brodsky, Phys. Rev. B **11**, 2271 (1975).

[26]D. Bermejo and M. Cardona, J. Non-Cryst. Solids **32**, 495 (1975).

[27]The analysis of a related light scattering phenomenon in chiral systems is presented in P. W. Higgs, Proc. R. Soc. London, Ser. A **220**, 472 (1953).

[28]Y. R. Shen, *The Principles of Non-Linear Optics* (Wiley, New York, 1985).

[29]E. Burstein and A. Pinczuk, *The Physics of Opto-Electronic Materials,* edited by Walter A. Albers, Jr. (Plenum, New York, 1971), p. 33.

[30]J. F. Nye, *Physical Properties of Crystals: Their Representation by Tensors and Matrices* (Clarendon, Oxford, 1957).

[31]L. D. Landau, E. M. Lifshitz, and L. P. Pitaevskii, *Electrodynamics of Continuous Media,* 2nd ed. (Pergamon, Oxford, 1984), p. 362

[32]*The New Encyclopedia Brittanica,* 15th ed. (The Encyclopedia Brittanica, Chicago, 1986), Vol. 1, p. 529.

[33]J. L. Oudar, A. Migus, D. Hulin, G. Grillon, J. Etchepare, and A. Antonetti, Phys. Rev. Lett. **53**, 384 (1984).

[34]W. A. Harrison, *Electronic Structure and the Properties of Solids* (Freeman, San Francisco, 1980).

[35]B. F. Levine, Phys. Rev. B **7**, 2600 (1973).

[36]Sudhanshu S. Jha and N. Bloembergen, Phys. Rev. **171**, 891 (1968).

[37]Chung L. Tang, IEEE J. Quantum Electron. **QE-9**, 755 (1973).

[38]Gerald D. Mahan, *Many-Particle Physics* (Plenum, New York, 1981).

[39]S. Doniach and E. H. Sondheimer, *Green's Functions for Solid State Physics* (Benjamin, Reading, Mass., 1974).

[40]J. D. Jackson, *Classical Electrodynamics,* 2nd ed. (Wiley, New York, 1975), Chap. 4.

[41]J. D. Jackson, *Classical Electrodynamics,* 2nd ed. (Wiley, New York, 1975), Chap. 6.

[42]O. L. Alerhand and E. J. Mele, Phys. Rev. B **35**, 5533 (1987).

[43]D. J. Chadi, Phys. Rev. Lett. **43**, 43 (1979).

[44]D. J. Chadi, J. Vac. Sci. Technol. **16**, 1290 (1979).

[45]G. Leman and J. Friedel, J. Appl. Phys. **33**, 281 (1962).

[46]O. L. Alerhand, D. C. Allan, and E. J. Mele, Phys. Rev. Lett. **55**, 2700 (1985).

[47]D. C. Allan and E. J. Mele, Phys. Rev. Lett. **53**, 826 (1984).

[48]P. J. Steinhardt, D. R. Nelson, and M. Ronchetti, Phys. Rev. B **28**, 784 (1983).

[49]N. Bloembergen and P. S. Pershan, Phys. Rev. **128**, 606 (1962).

[50]J. D. Jackson, *Classical Electrodynamics,* 2nd ed. (Wiley, New York, 1975).

[51]J. A. Giordmaine, Phys. Rev. **138**, A1599 (1965).

[52]J. Jerphagnon, Phys. Rev. B **2**, 1091 (1970).

[53]Charles C. Wang, J. Bomback, W. T. Donlon, C. R. Huo, and J. V. James, Phys. Rev. Lett. **57**, 1647 (1986).

[54]D. J. Moss, H. M. van Driel, and J. E. Sipe, Appl. Phys. Lett. **48**, 1150 (1986).

[55]An experimental study of second-harmonic generation in optical fibers may be found in Ulf Osterberg and Walter Margulis, Opt. Lett. **12**, 57 (1987); **11**, 516 (1986).

[56]A related analysis of Raman scattering may be found in R. Loudon, Proc. R. Soc. London, Ser. A **275**, 218 (1963).

[57]John P. Carini, K. A. Muttalib, and Sidney R. Nagel, Phys. Rev. Lett. **53**, 102 (1984).

[58]V. P. Sukhatme and P. A. Wolff, Phys. Rev. Lett. **35**, 1369 (1975).

[59]N. D. Mermin, Phys. Rev. B **1**, 2362 (1970).